NOTES AND CORRESPONDENCE

Vertical Heat Fluxes Generated by Mesoscale Atmospheric Flow Induced by Thermal Inhomogeneities in the PBL

G. A. DALU

CIRA—Colorado State University, Fort Collins, Colorado
IFA-CNR, Rome, Italy

R. A. PIELKE

Department of Atmospheric Science, Colorado State University, Fort Collins, Colorado

8 November 1991 and 6 May 1992

ABSTRACT

An analytical evaluation of the vertical heat fluxes associated with the mesoscale flow generated by thermal inhomogeneities in the PBL in the absence of a synoptic wind is presented. Results show that the mesoscale fluxes are of the same order as the diabatic heat fluxes.

In the sea-breeze case results show that in the lower layer of the atmosphere the heat flux is positive over the land and negative over the sea with an overall positive horizontal average. In the free atmosphere above the PBL the mesoscale vertical heat flux is negative over the land and over the sea; that is, the lower atmosphere becomes warmer while the free atmosphere above becomes cooler. As a result the mesoscale flow contributes to the weakening of the atmospheric stability within a region that extends a Rossby radius distance from the coastline, and up to an altitude larger than twice the depth of the convective PBL. The average momentum flux equals zero because the momentum removed over the sea is fed back into the atmosphere over the land.

Sinusoidally periodic thermal inhomogeneities induce periodic atmospheric cells of the same horizontal scale. The intensity of mesoscale cells increases for increasing values of the wavenumber, reaches its maximum value when the wavelength of the forcing is of the order of the local Rossby radius, and then decreases as the wavelength of the forcing decreases, because of the destructive interference between mesoscale cells. The intensity of the vertical velocity and vertical fluxes is, however, only a weak function of the wavenumber, at large wavenumber. Therefore, the intensity of the mesoscale heat flux does not decrease substantially at high wavenumbers; however, the transport of cool air over small heated patches of land may cut off the temperature gradient in the atmosphere between the land and water early in the day, thereby reducing the duration of the mesoscale activity. Also horizontal diffusion of heat in the convective boundary layer can significantly weaken horizontal temperature gradients for large wavenumbers. Periodic square-wave thermal inhomogeneities are more effective than sinusoidal waves in generating mesoscale cells; that is, the intensity of the flow is generally stronger. When dealing with low resolution models, which do not resolve explicitly the mesoscale activity, the mesoscale heat fluxes have to be introduced in a parametric form, using this or a similar theory.

1. Introduction

It has long been recognized that land and sea contrasts produce sea breezes (e.g., Pielke 1974). More recently, it has become evident that landscape variations that result in spatial gradients in surface heat flux can produce mesoscale circulations as strong as sea breezes (e.g., Ookouchi et al. 1984; Segal et al. 1988; Avissar and Pielke 1989); however, it remains to determine how small a horizontal variation in surface heating can still produce a significant mesoscale circulation.

In order to address this question, in this paper we present results from an analytic model. While only the linear response can be evaluated using this tool, such models have been shown to be effective at identifying dominant physical processes associated with sea breezes (e.g., Rotunno 1983; Dalu and Pielke 1989). This approach can also be used to assist in the development of a parameterization of mesoscale effects generated by spatial surface sensible heat variability for use in larger-scale models. We use Laplace transform theory for the time behavior and Green function theory for the spatial structure.

2. Governing equation and atmospheric response

From Rotunno (1983), thermally forced atmospheric flow, in the absence of a large-scale wind, can be reduced to a single equation for the streamfunction. Using the notations given in Dalu and Pielke (1989),

Corresponding author address: Dr. Roger A. Pielke, Department of Atmospheric Sciences, Colorado State University, Fort Collins, CO 80523.

the Laplace-transformed nondimensional equation for the streamfunction can be written as

$$\frac{\partial^2}{\partial\hat{\xi}^2}\hat{\psi}+\frac{\partial^2}{\partial\hat{\eta}^2}\hat{\psi}=-\hat{\beta}(p)\frac{\partial}{\partial\hat{\xi}}\hat{Q}, \tag{2.1}$$

$$\hat{\beta}(p)=\left(\frac{1}{\tilde{N}^2+p^2}\right)^{1/2}\left(\frac{1}{\tilde{f}^2+p^2}\right)^{1/2}\approx\frac{1}{\tilde{N}}\frac{1}{\sqrt{\tilde{f}^2+p^2}}. \tag{2.2}$$

We assume that the terrain is flat and that the vertical velocity vanishes at the ground:

$$w(x, z=0, t)=\tilde{w}(\tilde{\xi}, \tilde{\eta}=0, \tau)$$
$$=\hat{w}(\hat{\xi}, \hat{\eta}=0, s)=0. \tag{2.3}$$

The Green function for the Poisson equation (2.1) in the upper semiplane, which satisfies the boundary condition, Eq. (2.3), is

$$\hat{g}_\psi=-\frac{1}{2\pi}\ln\left[\frac{(\hat{\xi}-\hat{\xi}')^2+(\hat{\eta}+\hat{\eta}')^2}{(\hat{\xi}-\hat{\xi}')^2+(\hat{\eta}-\hat{\eta}')^2}\right]^{1/2}. \tag{2.4}$$

The variables with the tilde (˜) are nondimensional; the variables with the hat (ˆ) are Laplace transformed; s is the Laplace transform variable related to the nondimensional time τ:

$$\tau=tT^{-1};\quad \hat{\eta}=\frac{z}{\bar{h}};\quad \hat{\xi}=\frac{x}{\bar{R}};\quad p=s+\tilde{\lambda}. \tag{2.5}$$

The relation between the buoyancy source Q and the diabatic heat flux ϕ is

$$-\frac{g}{\rho c_p\bar{\Theta}}\frac{\partial\phi(x, z, t)}{\partial z}=Q(x, z, t)=Q_0r(x, z)q(t). \tag{2.6}$$

The vertical and horizontal scales (Green and Dalu 1980; Dalu et al. 1991) are

$$h=\frac{2Q_0}{N_0^2}\int_0^t dt'q(t');$$

$$R=N_0\int_0^t dt'h(t-t')\exp(-\lambda t')J_0(ft'). \tag{2.7}$$

We use the following values for the Brunt–Väisälä frequency N_0, Coriolis parameter f, and friction λ:

$$N_0=\left(g\frac{\Theta_z}{\Theta}\right)^{1/2}=10^{-2}\quad[\mathrm{s}^{-1}];\quad f=2\omega\sin\alpha$$
$$=O(10^{-4})\quad[\mathrm{s}^{-1}];\quad \omega=\frac{2\pi}{\mathrm{day}},\quad \lambda=O(\omega).$$

With these values of the characteristic time scale, asymptotic height of the PBL, h_0, and asymptotic Rossby radius R_0,

$$T=\frac{1}{\sqrt{f^2+\lambda^2}}=O(10^4)\quad[\mathrm{s}];$$

$$h_0=h(t_0)=1500\quad[\mathrm{m}];$$

$$R_0=R(t_0)=h_0\frac{N_0}{\sqrt{f^2+\lambda^2}}=100\quad[\mathrm{km}].$$

When a region experiences a warming γ times stronger than an adjacent one, in Eq. (2.6) we have

$$\frac{\partial r(x, z)}{\partial x}=\gamma\delta(x)\,\mathrm{He}(h_0-z). \tag{2.8}$$

Here He is the Heaviside function and δ is the Dirac function. Through inverse Laplace transform, the atmospheric response is

$$\hat{\psi}=\gamma\tilde{Q}_0\hat{q}(s)\hat{\beta}(p)\hat{G}_\psi(\hat{\xi}, \hat{\eta})\Rightarrow\psi(x, z, t)$$
$$=\frac{\gamma Q_0h_0}{T}\langle q(t)\times\{\exp(-\lambda t)[J_0(ft)$$
$$\times(J_0(N_\gamma t)\times G_\psi(x, z))]\}\rangle$$
$$\approx\frac{\gamma Q_0h_0}{TN_\gamma}\{q(t)\times[\exp(-\lambda t)(J_0(ft)\times G_\psi(x, z))]\},$$

$$\hat{G}_\psi(\hat{\xi}, \hat{\eta})=\int_0^{\hat{h}}d\hat{\eta}'\int_{\hat{r}}d\hat{\xi}'\frac{\partial\hat{r}}{\partial\hat{\xi}'}\hat{g}_\psi(\hat{\xi}-\hat{\xi}', \hat{\eta}-\hat{\eta}')$$
$$\approx\hat{H}_\psi(\hat{\eta})\exp(-|\hat{\xi}|). \tag{2.9}$$

Given the structure of the Green function [Eq. (2.4)], the intensity of the perturbation decays as the logarithm of the ratio between distance from the source $(\hat{\xi}', \hat{\eta}')$ and from its mirror image $(\hat{\xi}', -\hat{\eta}')$. (The perturbation is confined to the neighborhood of the source and of its image.) The eventual presence of complex poles in inverting Eq. (2.9), however, gives rise to oscillations in time–space, that is, damped propagating waves referred to in the literature as front runners (Geisler and Bretherton 1969). Furthermore, Sun and Orlanski (1981) have shown that some modes can become unstable for some values of the pulsation and the wavenumber (complex poles with positive real part). We will not treat the problem in such general terms; the case when $\hat{\xi}$ becomes imaginary under sinusoidal in time forcing has been treated by Rotunno (1983); the case when $\hat{\xi}$ is complex has been examined by Dalu and Pielke (1989).

In physical space and asymptotically in time G_ψ becomes

$$G_\psi(x, z)\approx H_\psi(z)\exp\left(-\left|\frac{x}{R_\gamma}\right|\right),$$

$$H_\psi(z)=\frac{1}{2\pi}\left\{\frac{z}{h_0}\ln\left|\frac{z^2-h_0^2}{z^2}\right|+\ln\left|\frac{z+h_0}{z-h_0}\right|\right\}, \tag{2.10}$$

$$G_u(x, z) = h_0 \frac{\partial G_\psi(x, z)}{\partial z},$$

$$G_w(x, z) = -R_\gamma \frac{\partial G_\psi(x, z)}{\partial x}.$$

The flow intensity decays exponentially with an e-folding distance equal to the Rossby radius from an abrupt variation in diabatic heat flux (Dalu et al. 1991); we will use this approximation in computing the horizontally averaged vertical fluxes. Also

$$\hat{\eta} = \frac{z}{h_0}, \quad \hat{\xi} = \frac{x}{\hat{R}_\gamma}, \quad N_\gamma^2 = |\gamma| N_0^2,$$

$$R_{0_\gamma} = h_0 \left(\frac{N_\gamma^2 + \lambda^2}{f^2 + \lambda^2}\right)^{1/2} \approx h_0 \frac{N}{\sqrt{f^2 + \lambda^2}},$$

where R_{0_γ} is the asymptotic *local Rossby radius.* The atmospheric response is a convolution of damped trapped inertia-gravity waves, written in terms of Bessel functions, trigonometric functions, and exponentials (Dalu and Pielke 1989). Here $\{\times\}$ denotes the convolution product in time; the evolution is reconstructed through the use of the Faltung theorem (Fodor 1965).

3. Heat and momentum fluxes in a sea-breeze case

The sea-breeze flow, Fig. 1, reaches its mature state when $t = t_0 = 0.5$ [day] $\approx 4T$. In the forcing equation (2.6) $r(x, z)$ is

$$r(x, z) = \left[\frac{x\,\mathrm{He}(x) - (x - L)\,\mathrm{He}(x - L)}{L}\right] \times \mathrm{He}(h_0 - z), \quad (3.1)$$

where L is a transition region near the coast, where the diabatic warming is assumed less intense because of the horizontal advection of cool air:

$$L = \frac{1}{h_1}\int_0^{h_1} dz \int_0^{t_0} u dt' = h_0 T N_0 = \frac{R_0}{4};$$

$$h_1 = \frac{h_0\sqrt{2}}{2}; \quad \frac{1}{h_1}\int_0^{h_1} dz H_u = \frac{1}{4}.$$

At $z = h_1$, the mesoscale flow reverses its direction (Fig. 1b). The asymptotic streamfunction, horizontal, and vertical momentum components (Fig. 1a,b,c) are

$$\psi = \psi_0 \int_{-\infty}^{-\infty} dx' g_\psi(x - x', z) \frac{\partial r(x', z)}{\partial x};$$

$$u = \frac{\partial \psi}{\partial z}, \quad w = -\frac{\partial \psi}{\partial x}.$$

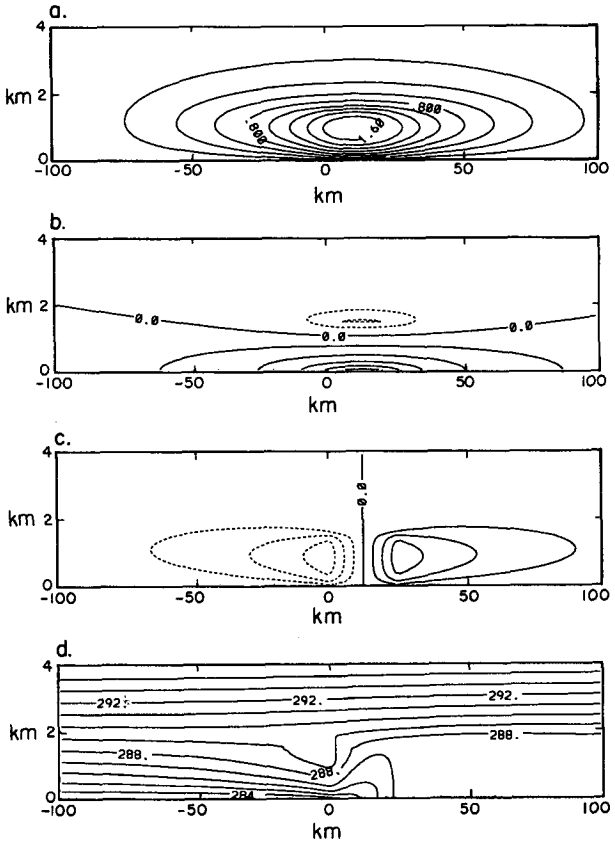

FIG. 1. Sea-breeze flow in a mature state. (a) Streamfunction ψ, $\Delta\psi = 0.2$ [10^3 m^2 s^{-1}], 40° of latitude ($\lambda = \omega$), $h_0 = 1500$ m, $R_0 = 100$ km. (b) Horizontal momentum component u, $\Delta u = 1$ [m s^{-1}]. (c) Vertical momentum component w, $\Delta w = 1$ [cm s^{-1}]. (d) Potential temperature θ, $\Delta\theta = 1$ [K].

The asymptotic amplitudes are

$$\psi_0 = \frac{Q_0 h_0 t_0}{N_0} = \frac{N_0 h_0^2}{2} = \frac{R_0 h_0}{2T}; \quad u_0 = \frac{\psi_0}{h_0} = \frac{N_0 h_0}{2} = \frac{R_0}{2T}; \quad w_0 = u_0 \frac{h_0}{R_0} = \frac{\psi_0}{R_0} = \frac{h_0}{2T}. \quad (3.2)$$

The temperature perturbation (Fig. 1d) is

$$\theta = \theta_D - \left[\frac{\partial \theta_D}{\partial z} + (1 - r(x, z))\Theta_z\right]\Delta_z;$$

$$\theta_D = r(x, z)(h_0 - z)\Theta_z;$$

$$\Delta_z(x, z, t_0) = \int_0^{t_0} dt' w(x, z, t'),$$

where Θ_z is the vertical gradient of potential temperature in the environment. The first term θ_D is the diabatically induced temperature perturbation; the second term is the temperature perturbation due to the linear

mesoscale advection; Δ_z is the vertical particle displacement. An estimate of the heat flux carried by the mesoscale circulation is $(w_0 - w_D)\theta$, where w_0 is given in Eq. (3.2) and w_D is the vertical velocity if it were entirely due to diabatic heating:

$$w_D = \frac{Q_0}{N_0^2} = \frac{h}{2\int_0^t dt' q(t')} \approx \frac{h}{2\bar{T}},$$

where $\bar{T}$ is the diabatic heat time scale. The time-dependent diabatic vertical heat flux over the ocean is zero; over the heated land and within the PBL the diabatic vertical heat flux is positive and time dependent (3.1); its horizontal average is positive:

$$\bar{F}_D = (h_0 - z)\frac{h_0\Theta_z}{2t_0}\frac{q(t)}{2R_0 + L}\int_{-R_0}^{R_0+L} dx r(x, z) = (h_0 - z)\frac{q(t)h_0\Theta_z}{4t_0}. \quad (3.3)$$

The mesoscale vertical heat flux within the PBL over the land is positive and is negative over the ocean; the horizontally averaged mesoscale heat flux is positive in the lower atmosphere and negative aloft:

$$\bar{F}_{M\theta} = \frac{1}{2R_0 + L}\int_{-\infty}^{\infty} dx\theta w = \frac{w_0\Theta_z}{2R_0 + L} \times \left\{ \mathrm{F}_0(t)F_1(t)(h_0 - z)\int_{-\infty}^{\infty} dx r(x, z)G_w(x, z) + F_0(t)F_1(t)F_2(t)w_0\int_{-\infty}^{\infty} dx r(x, z)G_w^2(x, z) - F_1(t)F_2(t)w_0\int_{-\infty}^{\infty} dx G_w^2(x, z)\right\}. \quad (3.4)$$

The vertical profiles of the diabatic and the mesoscale heat fluxes and the diabatic and mesoscale heating rates, in the mature state presented in Fig. 1, are shown in Fig. 2c. The time functions in Eq. (3.4) are

$$F_0(t) = 2\mathcal{L}^{-1}\left\{\frac{\hat{q}(s)}{p}\right\}; \quad F_1(t) = \mathcal{L}^{-1}\{\hat{q}(s)\hat{\beta}(p)\}; \quad F_2(t) = \mathcal{L}^{-1}\left\{\frac{\hat{q}(s)\hat{\beta}(p)}{p}\right\},$$

where $\mathcal{L}^{-1}$ is the inverse Laplace transform. Here $F_0(t)$ is representative of the evolution of the diabatic temperature perturbation [$q(t)$ is the time behavior of the diabatic heat flux]; $F_1(t)$ shows the evolution of the amplitude of the streamfunction, the horizontal and vertical velocity, and the horizontal scale; and $F_2(t)$ illustrates the evolution of the amplitude of particle displacement, that is, the temperature evolution in the stratified region of the atmosphere. The time behavior of these functions and of the mesoscale heat flux, $\bar{F}_{M\theta}(z = 500\text{ m}, t)$, is shown in Fig. 2a for the sinusoidal forcing, $q(t) = \pi/2\sin(\omega t)$. For an impulsive forcing $q(t) = \mathrm{He}(t)$ (Fig. 2b), as for the case of cold air advected over a differentially heated region. For sinusoidal in time forcing, the mesoscale atmospheric cells reach their maturity in about 1/3 day, which is also the time required to reach the balance between the forcing and the dissipation in the case of impulsive in time forcing. This last information is useful when the present theory is used in models that do not resolve the diurnal cycle.

Thus, the sea-breeze-generated fluxes are of the same order as the diabatic contribution; therefore, the sea-breeze thermal perturbation obviously cannot be neglected in coastal areas. This result is not surprising. We have known for years that realistic simulations of coastal environments must consider sea breezes when the synoptic winds are light (Walsh 1974). In section 4, however, we will demonstrate that this effect is likely to be equally important over inland areas.

Inspecting the structure functions [G_u] and [G_w] and Fig. 1b and 1c, we see that the vertical velocity is an antisymmetric function of the horizontal coordinate while the horizontal velocity is a symmetric function. Therefore, the vertical momentum flux associated with the mesoscale flow can differ from zero only locally, and its horizontal average equals zero, $\bar{F}_u = 0.0$. The amount of horizontal momentum fed into the free atmosphere over the heat patch is removed over the ocean:

$$\vec{F}_u = \frac{1}{R_0}\int_0^{\infty} uv dx = -\overleftarrow{F}_u = -\frac{1}{R_0}\int_{-\infty}^{0} uv dx, \qquad \bar{F}_u = \frac{\vec{F}_u + \overleftarrow{F}_u}{2} = 0. \quad (3.5)$$

The *vertical flux* of horizontal momentum, when horizontally averaged, is *negligible.* In addition, from Eq. (3.2) we deduce that

$$\frac{\partial}{\partial t} = \mathrm{O}\left(\frac{1}{T}\right), \quad u\frac{\partial}{\partial x} = \mathrm{O}\left(\frac{u_0}{R_0}\right) = \mathrm{O}\left(\frac{1}{2T}\right); \quad \text{and} \quad w\frac{\partial}{\partial z} = \mathrm{O}\left(\frac{w_0}{h_0}\right) = \mathrm{O}\left(\frac{1}{2T}\right); \quad (3.6)$$

that is, the advection terms are smaller than the linear term but of the same order. Thus, the linear theory underestimates the perturbations predicted by a nonlinear theory. A first-order estimate of the nonlinear contribution of the heat flux fed into the free atmosphere is

$$\mathrm{He}(z - h_0)\bar{F}_\theta = \frac{1}{2R_0}\int_{-\infty}^{\infty} dx w\Delta_z\frac{\partial\theta}{\partial z} = \frac{1}{2R_0}\int_{-\infty}^{\infty} dx\Delta_z\frac{d\Delta_z}{dt}\frac{\partial\theta}{\partial z} = 0;$$

that is, $\mathrm{He}(z - h_0)\bar{F}_\theta$ vanishes in the average (the integrand is antisymmetric because $[\Delta_z d\Delta_z/dt]$ is sym-

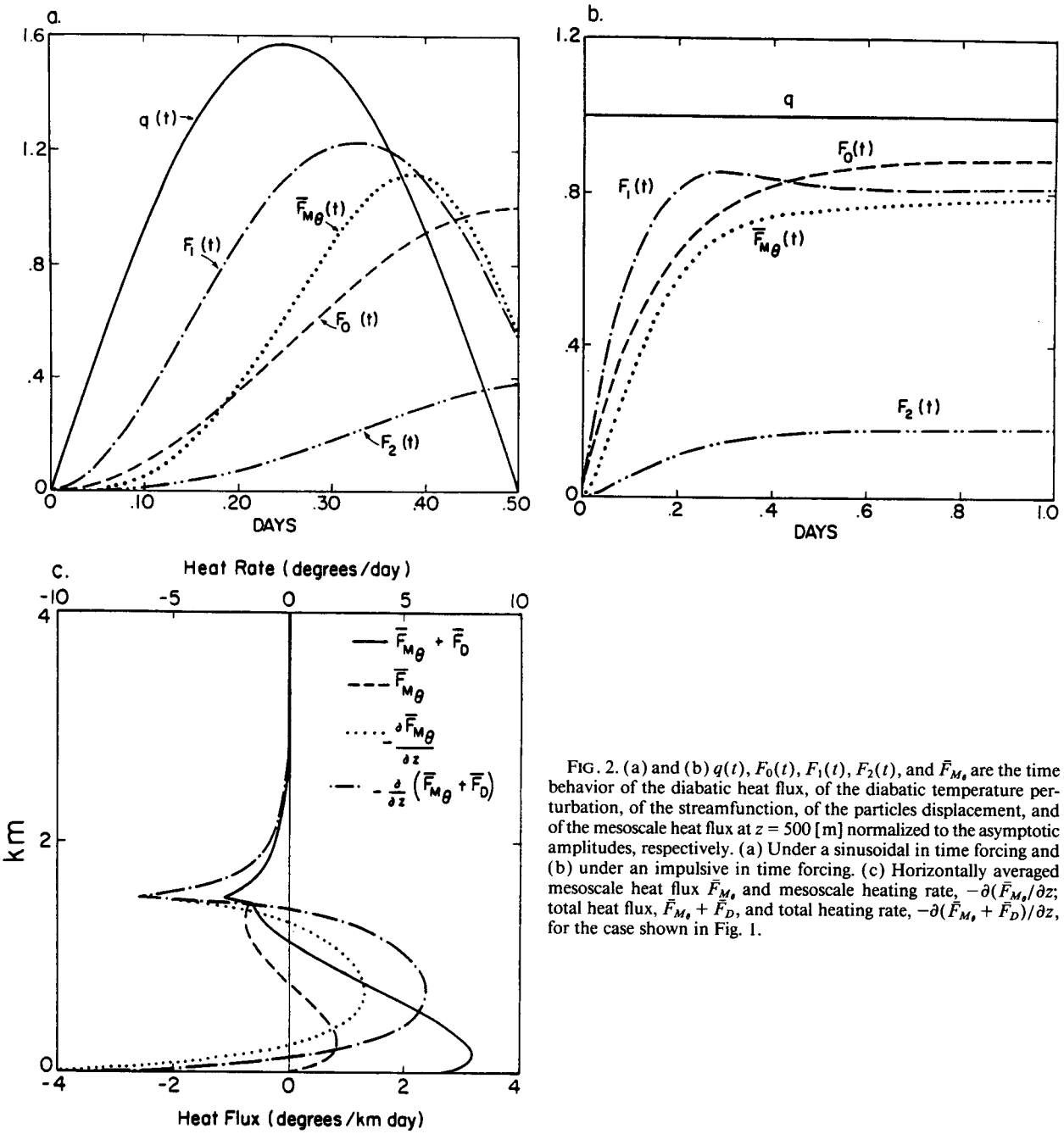

FIG. 2. (a) and (b) $q(t)$, $F_0(t)$, $F_1(t)$, $F_2(t)$, and $\bar{F}_{M_\theta}$ are the time behavior of the diabatic heat flux, of the diabatic temperature perturbation, of the streamfunction, of the particles displacement, and of the mesoscale heat flux at $z = 500$ [m] normalized to the asymptotic amplitudes, respectively. (a) Under a sinusoidal in time forcing and (b) under an impulsive in time forcing. (c) Horizontally averaged mesoscale heat flux $\bar{F}_{M_\theta}$ and mesoscale heating rate, $-\partial(\bar{F}_{M_\theta}/\partial z$; total heat flux, $\bar{F}_{M_\theta} + \bar{F}_D$, and total heating rate, $-\partial(\bar{F}_{M_\theta} + \bar{F}_D)/\partial z$, for the case shown in Fig. 1.

metric and $[\partial\theta/\partial z]$ is antisymmetric). The nonlinear advection, however, may break the symmetry, and the structure functions may not be exactly symmetric or antisymmetric. For a quantitative evaluation of the nonlinear contributions see the paper by Pielke et al. (1991).

4. Heat fluxes under periodic diabatic forcing

When the diabatic heat is sinusoidally periodic with L_m as the wavelength,

$$Q = Q_0 q(t)\,\mathrm{He}(h_0 - z)\left[\frac{1}{2} + \frac{1}{2}\sin\left(\frac{m\pi x}{R_0}\right)\right];$$

$$m = \frac{2R_0}{L_m}.$$

This situation could correspond to inland patches of periodically heated land, such as regions of landscape variability. The streamfunction and the horizontal velocity are

$$\psi = \psi_{0_m} H_\psi(z) \cos\left(\frac{m\pi x}{R_0}\right); \quad \psi_{0_m} = \psi_0 \frac{m\pi}{(m\pi)^2 + 1}$$

$$u = u_{0_m} H_u(z) \cos\left(\frac{m\pi x}{R_0}\right); \quad u_{0_m} = u_0 \frac{m\pi}{(m\pi)^2 + 1}.$$

Here m is the number of wavelengths in a $2R_0$ distance (m need not be integer). The streamfunction isolines for $m = 1$ and $m = 2$ are shown in Fig. 3a and Fig. 3c. The intensity of the flow ψ_{0_m} decays as $1/(\pi m)$ at high wavenumbers (Fig. 4a). The vertical velocity is

$$w = w_{0_m} H_w(z) \sin\left(\frac{m\pi x}{R_0}\right); \quad w_{0_m} = w_0 \frac{(m\pi)^2}{(m\pi)^2 + 1}. \tag{4.1}$$

At higher wavenumbers, $m > 1$, the vertical velocity is a weak function of the wavenumber (Fig. 4b). The temperature perturbation, Fig. 3b and Fig. 3d, is

$$\theta = \theta_D - \frac{\partial \theta_D}{\partial x} \Delta_x - \left[\frac{\partial \theta_D}{\partial z} + (1 - r(x, z))\Theta_z\right]\Delta_z;$$

$$\theta_D = r(x, z)(h_0 - z)\Theta_z.$$

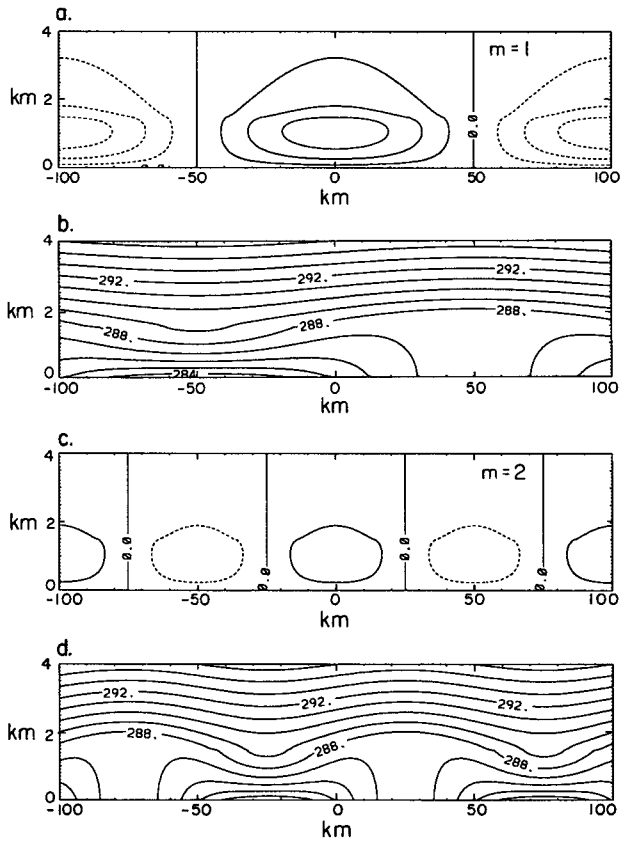

FIG. 3. Streamlines, $\Delta\psi = 0.2$ [10^3 m^2 s^{-1}], solid lines are positive, and dashed lines are negative. Potential temperature isolines, $\Delta\theta = 1$ [K], for two values of the horizontal wavenumber ($m = 1, 2$) for a horizontally sinusoidal periodic diabatic forcing.

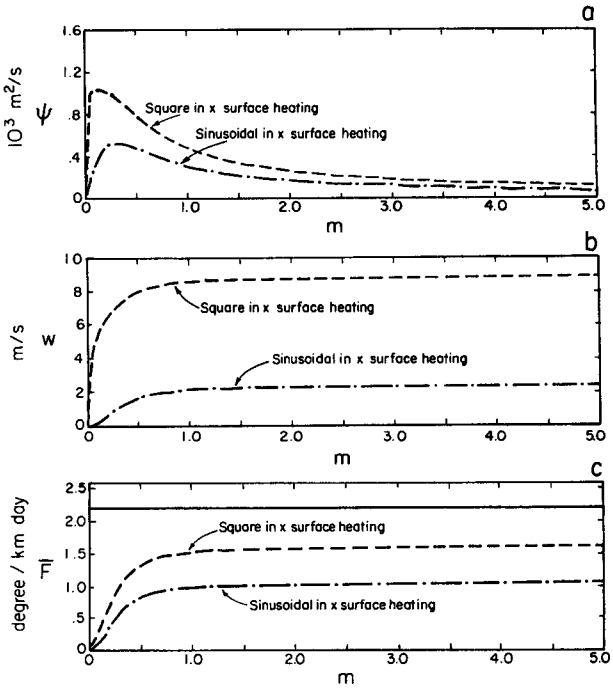

FIG. 4. (a) Intensity of the flow ψ_{0_m} induced by a sinusoidal (dash–dotted line) and by a square periodic forcing (dashed line) versus horizontal wavenumber m. (b) Vertical velocity w_{0_m} for a sinusoidal (dash–dotted line) and for a square periodic forcing (dashed line). (c) Flux intensities at $z = 500$ [m]; diabatic heat flux $\bar{F}_D$ (solid line); mesoscale heat flux $\bar{F}_{M_\theta}$ for a sinusoidal (dash–dotted line) and for a square periodic forcing (dashed line).

The vertical profile of the time-dependent mesoscale heat flux for a sinusoidal forcing, averaged over a wavelength, is

$$\bar{F}_{M_\theta} = \langle \theta w \rangle_{L_m} = \mathrm{He}(h_0 - z) w_0 H_w(z) \left[\frac{(m\pi)^2}{(m\pi)^2 + 1}\right] \times \left[\frac{(h_0 - z)\Theta_z}{4}\right] F_0(t) F_1(t) - \left[\frac{1}{2} - \frac{\mathrm{He}(h_0 - z) F_0(t)}{4} + \frac{\mathrm{He}(z - h_0)}{2}\right] \times \left[w_0 H_w(z) \frac{(m\pi)^2}{(m\pi)^2 + 1}\right]^2 \Theta_z F_1(t) F_2(t). \tag{4.2}$$

The mesoscale heat flux amplitude as a function of the wavenumber is shown in Fig. 4c. The vertical profile of the horizontally averaged mesoscale heat flux and the corresponding heating rate are shown in Fig. 5a for wavenumber $m = 4$. The time behavior of the mesoscale vertical heat flux is similar to the ones shown in Fig. 2a and 2b. The mesoscale heat flux does not decay at high wavenumber; this result is confirmed by numerical simulations for heat patches of 8 km or greater (Pielke et al. 1991).

When the forcing is a periodic square wave over the entire horizontal domain, with L_m as the wavelength:

$$Q = Q_{0q}(t)\,\mathrm{He}(h - z) \times \left[\frac{1}{2} + \frac{1}{2}\sum_{n=1,3\ldots}^{\infty} \frac{4}{n\pi}\sin\left(\frac{mn\pi x}{R_0}\right)\right];$$

$$m = \frac{2R_0}{L_m}. \quad (4.3)$$

The streamfunction is given by

$$\psi = \psi_0 H_\psi(z) \sum_{n=1,3\ldots}^{\infty} \frac{4}{n\pi}\frac{mn\pi}{(mn\pi)^2 + 1}\cos\left(\frac{mn\pi x}{R_0}\right). \quad (4.4)$$

The amplitude behavior of the streamfunction as a function of the wavenumber is shown in Fig. 4a. The vertical velocity, Fig. 4b, is

$$w = w_0 H_w(z) \sum_{n=1,3\ldots}^{\infty} \frac{4}{n\pi}\frac{(mn\pi)^2}{(mn\pi)^2 + 1}\sin\left(\frac{mn\pi x}{R_0}\right). \quad (4.5)$$

The average heat flux for a square periodic forcing is

$$\bar{F}_{M_\theta} = \langle \theta w \rangle_{L_m} = \mathrm{He}(h_0 - z) w_0 H_w(z)\frac{(h_0 - z)\Theta_z}{4} F_0(t)F_1(t) \sum_{n=1,3\ldots}^{\infty}\left(\frac{4}{n\pi}\right)^2 \frac{(mn\pi)^2}{(mn\pi)^2 + 1}$$
$$- \left[\frac{1}{2} - \frac{\mathrm{He}(h_0 - z)F_0(t)}{4} + \frac{\mathrm{He}(z - h_0)}{2}\right][w_0 H_w(z)]^2 \Theta_z F_1(t)F_2(t) \sum_{n=1,3\ldots}^{\infty}\left[\frac{4}{n\pi}\frac{(mn\pi)^2}{(mn\pi)^2 + 1}\right]^2. \quad (4.6)$$

The mesoscale heat flux amplitude as a function of the wavenumber is shown in Fig. 4c. The vertical profile of the horizontally averaged mesoscale heat flux and the corresponding heating rate for $m = 4$ are shown in Fig. 5b.

A physical mechanism that may control the amplitude of the mesoscale heat flux at very high wavenumbers is the transport of cold air over heated surface, which will eventually cut off the supply of sensible heat when

$$\int_0^t u_{0_m} dt' = \frac{L_m}{2} = \frac{R_0}{m},$$

but since u_{0_m} decays almost as $1/m$, the horizontal advection is a rather ineffective mechanism at high wavenumber. Another strong candidate is diffusion. If K_x is the horizontal diffusion coefficient, then the mesoscale activity is strongly reduced when

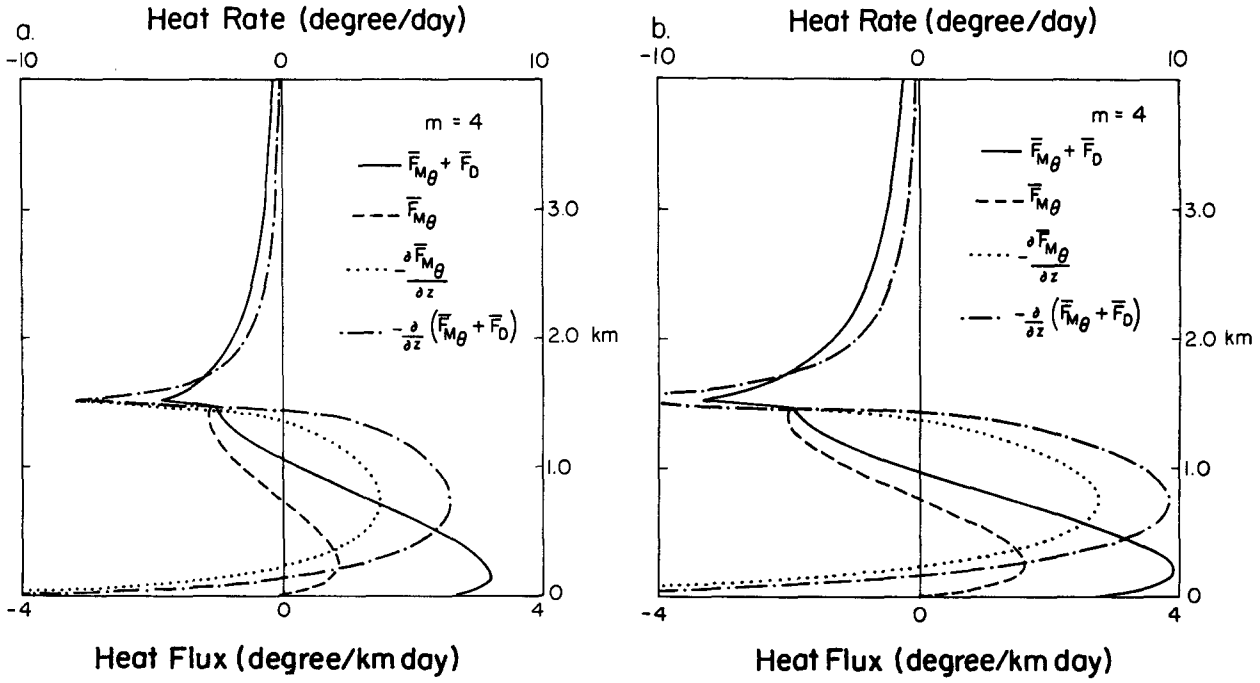

FIG. 5. (a) Horizonally averaged mesoscale heat flux and mesoscale heating rate for the case shown in Fig. 3c, sinusoidally periodic in space forcing. (b) Horizontally averaged mesoscale heat flux and mesoscale heating rate, as in 5a but for a square periodic in space forcing.

$$K_x\left(\frac{m\pi}{R_0}\right)^2 TF_1(t_m) = O(1),$$

$$\text{i.e., when} \quad m = \frac{1}{\pi}\left(\frac{N_0 h_0 R_0}{F_1(t_m)K_x}\right)^{1/2}.$$

At high wavenumber the mesoscale cells are active for a time $t = t_m$. If $K_x = 10\ m^2\ s^{-1}$, patches having a wavenumber $m = 100$ ($L_m = 2$ km) can be active until sunset, $t_m = t_0$. If $K_x = 100\ m^2\ s^{-1}$, only patches having a wavenumber $m \leq 30$ ($L_m = 7$ km) can be active until sunset. Patches having a wavenumber $m = 100$ ($L_m = 2$ km) can be active only for a tenth of that time, $t_m = 0.1t_0$; that is, the mesoscale activity becomes almost negligible, when the horizontal scale is of the same order of the vertical scale ($R_0/m \approx h_0$); Avissar and Pielke (1989) have assumed this result, without a justification as given here, in their parameterization of subgrid-scale landscape variations for use in a nonlinear mesoscale model.

5. Conclusions

Making use of the theory developed by Dalu and Pielke (1989), we deduce that, in the absence of larger-scale ambient flow, the vertical heat flux associated with mesoscale flow generated by horizontal surface thermal inhomogeneities, at least when horizontal diffusion effects and horizontal advection cannot eliminate the corresponding atmospheric thermal inhomogeneities, are of the same order as the turbulent diabatic heat flux, and therefore they cannot be neglected. These heat fluxes can have an intensity similar to sea breezes. To first order the vertical flux of horizontal momentum averages to zero. To first order, the mesoscale nonlinear contribution to heat flux above the PBL averages to zero, and therefore could be neglected to first order in a subgrid parameterization.

Square-wave periodic surface thermal inhomogeneities generate stronger atmospheric cells than sinusoidally distributed inhomogeneities. The intensity of the flow increases as the wavenumber increases, reaches its maximum when the wavelength is of the order of the Rossby radius, and then decreases linearly for large wavenumbers. Thus, significant atmospheric cells are generated by periodic thermal inhomogeneous patches only when the wavelength is a significant fraction of the local Rossby radius. When not resolved explicitly, the mesoscale heat fluxes can be introduced in parametric form using the present theory; however, it is unnecessary to resolve thermal inhomogeneities on scales much smaller than the local Rossby radius, because cool air transport over the convective region and horizontal diffusion reduces the amplitude of the mesoscale heat fluxes. In these cases the diabatic heat fluxes can be horizontally averaged beforehand, as applied in Avissar and Pielke (1989).

Solutions for the atmospheric perturbations in the presence of light ambient winds can be derived from the theory presented in this paper, and an extension of our theory in this direction is desirable. When the ambient flow is strong, however, the pattern of the perturbations can be quite different, as shown by Hsu (1987), and by Robichaud and Lin (1989) for atmospheric stationary perturbations. The simple analytical theory presented in this paper reproduces the qualitative behavior and the order of magnitude of the heat fluxes computed through a nonlinear numerical model with zero synoptic wind (Pielke et al. 1991).

Acknowledgments. We wish to thank Mike Moran for useful criticism and comments, and one of the reviewers for suggesting a scale analysis approach. We acknowledge the support of the National Science Foundation under Contract No. ATM-8915265. G. A. Dalu acknowledges the support of the Italian *CNR-ENEL* project.

REFERENCES

Avissar, R., and R. A. Pielke, 1989: A parameterization of heterogeneous land surfaces for atmospheric numerical models and its impact on regional meteorology. *Mon. Wea. Rev.*, **117**, 2113–2136.

Dalu, G. A., and R. A. Pielke, 1989: An analytic study of the sea breeze. *J. Atmos. Sci.*, **46**, 1815–1825.

——, ——, R. Avissar, G. Kallos, and A. Guerrini, 1991: Linear impact of subgrid-scale thermal inhomogeneities on mesoscale atmospheric flow with zero synoptic wind. *Ann. Geophys.*, **9**, 641–647.

Fodor, G., 1965: *Laplace Transform in Engineering.* Hungarian Academy of Science, 758 pp.

Geisler, J., and F. P. Bretherton, 1969: The sea breeze front runner. *J. Atmos. Sci.*, **26**, 82–95.

Green, J. A. S., and G. A. Dalu, 1980: Mesoscale energy generated in the boundary layer. *Quart. J. Roy. Meteor. Soc.*, **106**, 721–726.

Hsu Hsiao-Ming, 1987: Study of linear steady atmospheric flow above a finite surface heating. *J. Atmos. Sci.*, **44**, 186–199.

Ookouchi, Y., M. Segal, R. C. Kessler, and R. A. Pielke, 1984: Evaluation of soil moisture effects on the generation and modification of mesoscale circulation. *Mon. Wea. Rev.*, **117**, 2113–2136.

Pielke, R. A., 1974: A three-dimensional numerical model of the sea breezes over south Florida. *Mon. Wea. Rev.*, **102**, 115–139.

——, G. A. Dalu, J. S. Snook, T. J. Lee, and T. G. F. Kittel, 1991: Nonlinear influence of mesoscale land use on weather and climate. *J. Climate*, **4**, 1053–1069.

Robichaud, A., and C. A. Lin, 1989: Simple models of diabatically forced mesoscale circulations and mechanism of amplification. *J. Geophys. Res.*, **94**, 3413–3426.

Rotunno, R., 1983: On the linear theory of land and sea breeze. *J. Atmos. Sci.*, **40**, 1999–2009.

Segal, M., R. Avissar, M. C. McCumber, and R. A. Pielke, 1988: Evaluation of vegetation effects on the generation and modification of mesoscale circulations. *J. Atmos. Sci.*, **45**, 2268–2292.

Sun, W., and I. Orlanski, 1981: Large mesoscale convection and sea breeze circulation. Part I: Linear stability analysis. *J. Atmos. Sci.*, **38**, 1675–1693.

Walsh, J., 1974: Sea breeze theory and applications. *J. Atmos. Sci.*, **31**, 2012–2026.